Nano Research
2021, 14(3): 829–833

ISSN 1998-0124 CN 11-5974/O4
https://doi.org/10.1007/s12274-020-3120-2

Research Article

Heat dissipation in graphene foams

Yaniv Cohen, Siva K.Reddy, and Assaf Ya'akobovitz (✉)

Department of Mechanical Engineering, Faculty of Engineering Sciences, Ben-Gurion University of the Negev, Beer-Sheva 8410501, Israel

Received: 9 May 2020 / **Revised:** 29 July 2020 / **Accepted:** 15 September 2020

ABSTRACT

Graphene foam (GF)—a three-dimensional network of hollow graphene branches—is a highly attractive material for diverse applications. However, to date, the heat dissipation characteristics of GFs have not been characterized. To fill this gap, we synthesized GF devices, subjected them to high temperatures, and investigated their thermal behavior by using infrared microthermography. We find that while the convective area of GF devices is comparable to that of bulk materials (such as metals), the coefficient of convection of these devices is several orders of magnitude higher than that of metals. In addition, the GF devices showed a reproducible thermal behavior, which we attribute to negligible temperature-induced morphological changes (as confirmed by Raman analysis). Taken together, our findings suggest GF as a promising candidate material for advanced cooling applications where efficient heat dissipation is needed, e.g., in electrical circuits.

KEYWORDS

convection, graphene foam, heat transfer

1 Introduction

The miniaturization of electrically operated devices dramatically promotes their functionality and applicative potential; however, it also substantially increases their power density and subjects them to high electrical heat fluxes [1–5], requiring that they are constantly and effectively cooled [6]. While classical cooling methods [7–9], including convective cooling fins [1, 10–13], are still being used to cool miniaturized electrically operated devices, advanced nano-scale materials offer new frontiers for the thermal management of electrical components and other miniaturized systems, as they provide improved heat dissipation capacities. In this study, we investigate the possible use of one of the most promising nano-materials known today—graphene foam (GF)—as a high-end heat-dissipating material.

GF is a relatively new three-dimensional configuration of graphene, arranged as a network of hollow branches [14, 15]. Synthesizing the graphene in a three-dimensional formation yields new properties, such as high mechanical compliance [16] and a unique electromechanical signature [17]. As a result, GF has been integrated into various applications, including reinforcement for composites [18, 19], piezoresistive sensors [20], energy conversion devices [21], and resonators [22]. Thermally, GF composites show enhanced thermal conduction [19, 23] and an excellent ability to store thermal energy [24], while maintaining high mechanical flexibility [19]. Importantly, GF has also demonstrated low interface thermal resistance [25]—a property that strongly encourages its use in cooling applications.

However, despite the promising potential of using GF for thermal management, its heat dissipation characteristics have not been investigated. Here, we characterize, for the first time, the heat-convective properties of GF devices subjected to high temperature loading. We find that, while the convective area of GF is comparable to that of bulk materials, its coefficient of convection is high in comparison to its coefficient of conduction, indicating that it can operate as an excellent heat-dissipating component in advanced functional systems.

2 Methods

The GF devices (Fig. 1) were grown by chemical vapor deposition (CVD) on a commercially available porous nickel scaffold (95% porosity). The scaffold was inserted into a high-temperature tube furnace with a flow of ethylene gas (20 sccm for 15 min under 860 °C). During this process, the graphene was grown such that it covered the nickel and created the three-dimensional branches of the graphene. Then, the nickel was etched in HCl for 7 h, after which the devices were cleaned and dried. Energy dispersive X-ray spectroscopy (EDS) detected only negligible amounts of residual nickel in the devices (data are shown in the Electronic Supplementary Material (ESM)).

The devices were thermally characterized by infrared microthermography imaging, from which the temperature distribution was acquired along the height of the sample (Fig. 2(a)). Typically, in infrared measurements of bulk samples, the samples surface is perpendicular to the camera. In our system, due to the porous structure of the GF, only a small fraction of the surface is perpendicular, while most of the surface is tilted. As a result, the temperature readings are lower than their actual values. To overcome this challenge, we processed the temperature measurements to extract readings from parts of the surface that are perpendicular to the infrared camera, as explained below.

Due to the excellent thermal conduction of graphene sheets, we noticed that the thermal distribution of the GF devices depends only on their vertical coordinate, z. Namely, we used

Address correspondence to assafyaa@bgu.ac.il

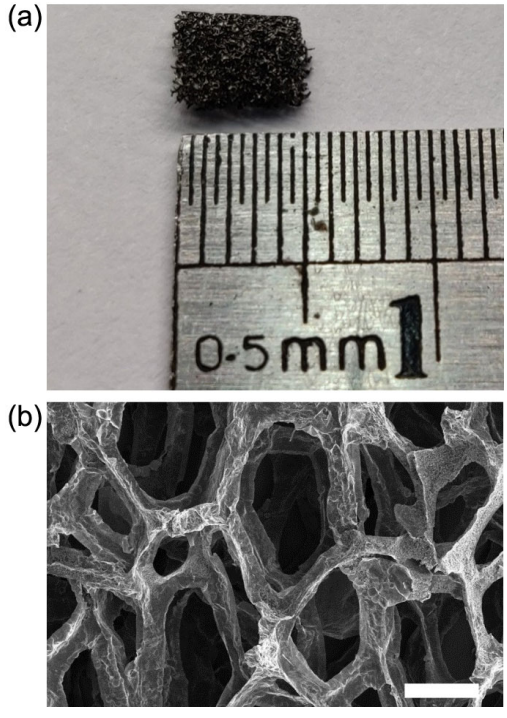

Figure 1 (a) Optical image of a representative GF device. (b) SEM micrograph of the GF. Scale bar: 200 μm.

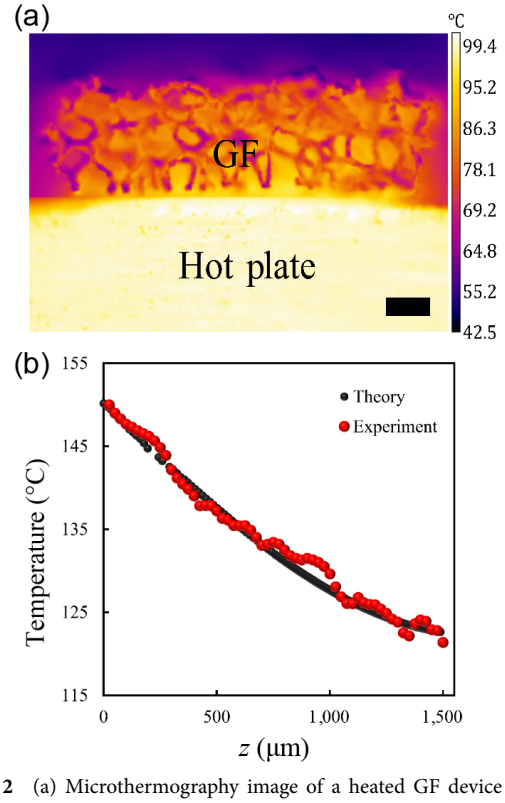

Figure 2 (a) Microthermography image of a heated GF device (device no. 2). Scale bar: 500 μm. (b) Measured (red markers) and calculated (black markers) temperature along the height of the sample.

a one-dimensional heat transfer assumption. For each horizontal line of pixels of the infrared image (namely, pixels with a fixed value of z), we averaged the temperature reading of only a small fraction of pixels (specifically, we chose 10% of the pixels, see discussion in the ESM) that presented the highest temperature readings. Indeed, this method yielded excellent agreement with the theoretical estimation of the temperature discussed below (Fig. 2(b)).

For the sake of simplicity, we normalized the temperature into a non-dimensional form, such that normalized temperature is $\theta(z) = (T(z) - T_\infty) / (T_w - T_\infty)$, where $T(z)$, T_∞, and T_w are the temperatures along the height of the devices, the environment temperature and the applied temperature at $z = 0$, respectively. The heat balance on a differentially thin cross-section yields the following differential equation

$$\frac{d^2\theta(z)}{dz^2} = m^2\theta(z) \quad (1)$$

where $m = \sqrt{hA_h / kA_k H}$. Note that h and k are the coefficients of convection and conduction, respectively. In addition, A_h, A_k and H represent the convective and conductive areas and the device height, respectively. The convective area is defined as the area from which heat is dissipated to the environment, while the conductive area is defined as the cross-section area from which heat is conducted along the height of the GF devices. As explained in our previous study [26], high A_h/A_k ratios indicate a significant convection, while $A_h/A_k \to 0$ indicates negligible convection. Under boundary conditions of fixed temperature at the bottom ($z = 0$) and convective cooling from the top ($z = H$), namely Newton boundary condition, the solution of Eq. (1) is given as

$$\theta(z) = \frac{m\cosh(m(H-z)) + h/k\sinh(m(H-z))}{m\cosh(mH) + h/k\sinh(mH)} \quad (2)$$

The ratios A_h/A_k and h/k, were extracted by numerically fitting the measured temperatures to Eq. (2). These values are shown in Fig. 3 and are discussed below.

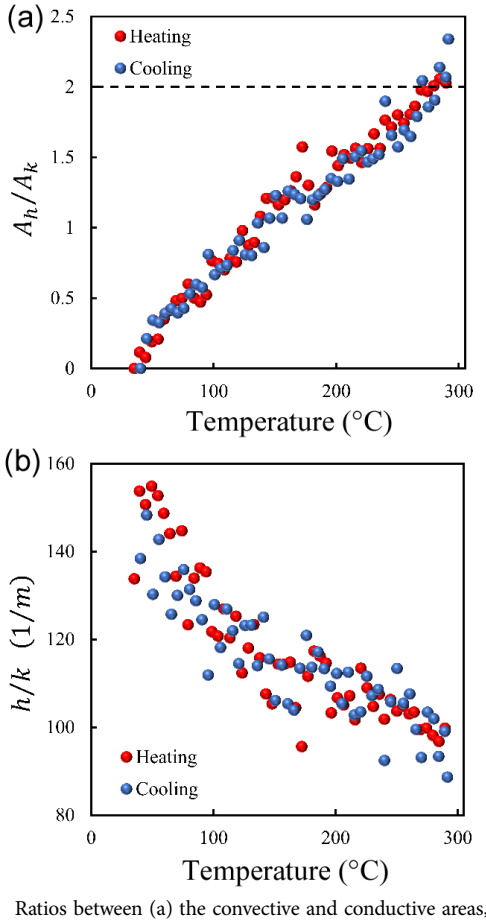

Figure 3 Ratios between (a) the convective and conductive areas, A_h/A_k (the dashed line corresponds to the ratio of a bulk material), and (b) the coefficients of thermal convection and conduction, h/k, of device no. 2 as a function of the applied temperature.

The Raman spectra of some devices were investigated both in room temperature and under high temperatures (devices were placed on a hot plate). Their Raman spectra were acquired as a function of the temperature.

3 Results and discussion

Several GF devices were synthesized and investigated, and all showed similar trends (for brevity, we provide here only the experimental data for device no. 2). Prior to heating—i.e., when the device temperature was equal to room temperature—the A_h/A_k ratio is zero (Fig. 3(a)), indicating that under ambient conditions the thermal convection in the GF devices is negligible. Heating the device increased the A_h/A_k ratio because it increased the kinetic energy of the air molecules, which increases the probability of thermally interacting with the device.

Despite the porous structure and the extremely high surface area of the GF devices, their A_h/A_k ratios, at high temperatures, are similar to those of bulk materials with the same dimensions (shown as a dashed line in Fig. 3(a); see also the ESM section). These relatively low A_h/A_k ratios are attributed to the open-cell foam structure of the GF–air molecules in interior pores of the GF require a long time to diffuse outside and dissipate the heat. Notably, carbon nanotube (CNT) forests also show a relatively low A_h/A_k ratio, but this is due to their nanoscale fibrous structure, which reduces the probability of air molecules interacting with the CNTs [26].

The ratio between the coefficients of thermal convection and thermal conduction (h/k), which expresses the relationship between the convective and conductive thermal resistances of the devices, decreased with increasing temperatures (Fig. 3(b)). Both coefficients increase with increasing temperatures, but the coefficient of conduction increases more significantly than the coefficient of convection, such that the h/k ratio decreases.

We defined the efficiency of the GF devices as the ratio between the heat that is transferred through the device and the heat that is transferred through an ideal thermal conductor (in which conductance is infinite). The efficiency of device no. 2 was ~ 0.83 (Fig. 4), which is comparable to that of metals, and indicates a low sensitivity to temperature.

The A_h/A_k ratio, the h/k ratio, and the efficiency of the devices (Figs. 3 and 4) were similar during heating and cooling, indicating that the thermal loading did not induce significant morphological changes. Furthermore, we also applied several thermal load cycles to a sample that demonstrated high reproducibility over the sequential loading cycles (see the ESM). In addition, Raman measurements (Fig. 5) acquired before and during the heating process (namely, at 150 °C and 300 °C) and again after the sample cooled to room temperature, revealed that the thermal loading did not shift the G- and 2D-Raman modes, which are highly sensitive to the morphological structure of the GF. Together with the reproducible results for the A_h/A_k and h/k ratios, these findings suggest that thermal loading does not induce morphological changes in the GF devices; this is in contrast to CNT forests, whose alignment is increased under thermal loads—resulting in significant morphological changes [27]. Importantly, both the reproducible thermal behavior of GF devices and their low morphological sensitivity to thermal loading are highly desired characteristics for functional thermal devices.

To demonstrate that the results of device 2 are not unique, in Fig. 6 we present the measurements from all of the devices examined in the framework of this study. We have chosen to present the data for an applied temperature of 150 °C. Relative to device no. 2 all devices exhibited similar A_h/A_k and h/k ratios, and similar efficiencies during heating and cooling, and were close to the average values recorded. The A_h/A_k ratio of most devices was ~ 1 (Fig. 6(a)), which is lower than that of bulk materials (e.g., metals) of the same dimensions (shown as a dashed line in Fig. 6(a)). The efficiency of all examined devices (Fig. 6(c)) was comparable to that of metals and CNT forests [26]. However and most importantly, the h/k ratios of GF are of the order of $h/k\big|_{GF} \sim 100m^{-1}$ (Fig. 6(b)). This value far exceeds that of bulk metals ($h/k\big|_{metal} \sim 0.1m^{-1}$, as demonstrated in the ESM where we compared the values of h/k of several bulk metals to that of GF).

Notably, while the qualitative behavior of all devices was similar, their A_h/A_k ratio, h/k ratio, and efficiency demonstrate some numerical scattering (Fig. 6), which we attribute mostly to morphological variance between the devices. The most influential morphological parameters in GF devices are the thickness of the graphene branches and the pore size and direction; although all devices were grown under the same conditions and from the same sheet of porous nickel scaffold, some variance in these two parameters can be expected.

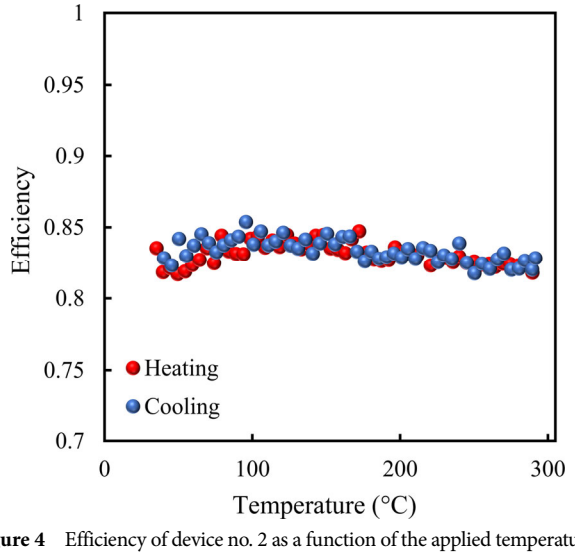

Figure 4 Efficiency of device no. 2 as a function of the applied temperature.

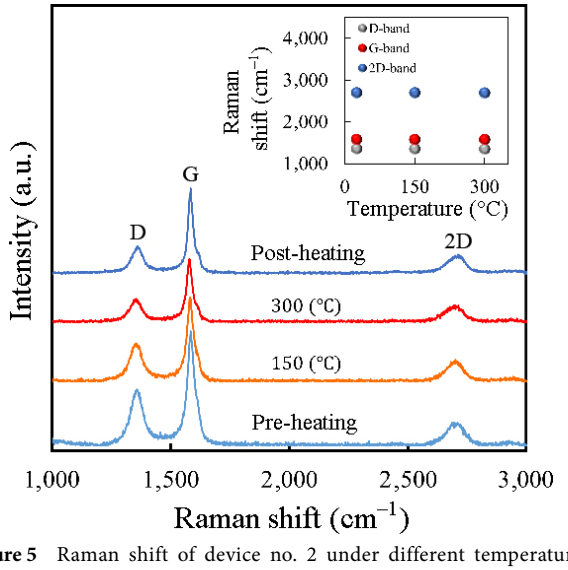

Figure 5 Raman shift of device no. 2 under different temperatures. Pre- and post-heating measurements were acquired at room temperature. Inset: Raman shifts of the D-, G-, and 2D-bands as a function of the temperature. Note that the pre- and post-heating shift measurements coincide.

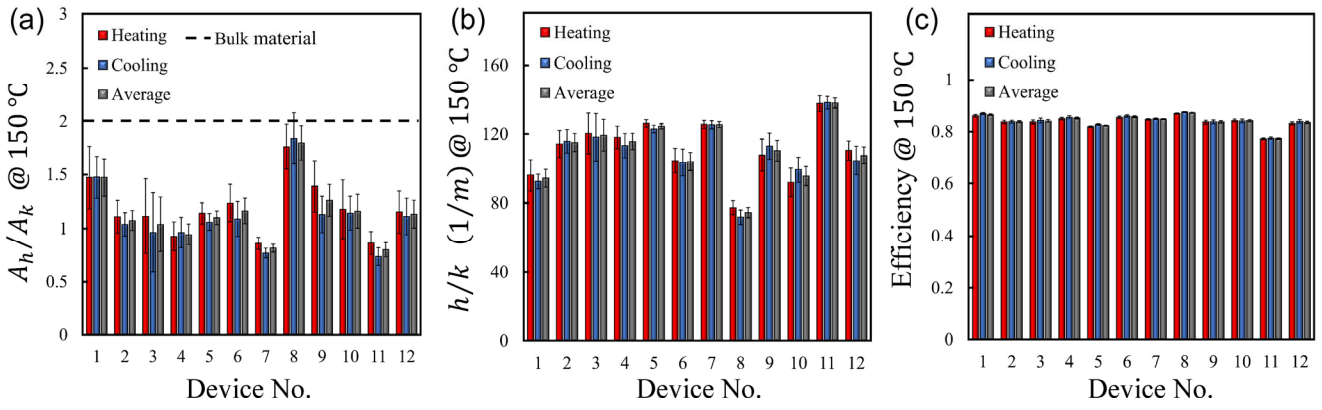

Figure 6 Results extracted from all investigated samples at 150 °C. (a) The ratios between the convective and conductive areas, A_h/A_k . The dashed line represents the A_h/A_k ratio of a bulk material. (b) The ratios between the coefficients of thermal convection and conduction, h/k . (c) The efficiency of the devices.

The coefficient of thermal conduction of GF devices was previously found to be in the order of $k_{GF} \sim 1\ W/mK$ [23]. Therefore, based on our measurements (e.g., Fig. 6(b)), the coefficient of thermal convection in these devices is in the order of $h_{GF} \sim 100\ W/m^2K$, which is very high for natural convection. We conducted finite-element analysis (FEA) simulations (using $k_{GF} = 1\ W/mK$, while $h_{GF} \sim 100\ W/m^2K$ was estimated from the calculation as detailed in the ESM) to simulate the thermal behavior of our GF devices. Simulations showed excellent agreement with the measured results, implying that the values of k_{GF} and h_{GF} can be reliably used to describe the thermal behavior of GF devices (Fig. 2(b)). In functional systems, the coefficient of thermal convection is often increased by adding air flow (i.e., a forced heat convection), but this solution dictates further complexity to the system because it requires large cooling fins, a fan, additional wiring, etc. Conversely, GF devices demonstrate a high coefficient of thermal convection under conditions of natural convection, which makes them highly attractive for use as cooling devices.

4 Conclusion

In this work, we have, for the first time, characterized the thermal dissipative behavior of GF devices. We find that the A_h/A_k ratio of these devices is low comparing to bulk material (due to slow diffusion of hot air molecules from the interior parts of the GF to the environment). In contrast, the h/k ratio is significantly larger than that of other materials—such as bulk metals—that are commonly used in cooling applications. An additional advantage of GF devices is that they demonstrate a highly reproducible thermal behavior due to negligible morphological changes when exposed to high temperatures.

The efficient cooling of electronic components is one of the greatest challenges toward their further minimization. Our findings that demonstrate high coefficient of convection, combined with the low thermal interface resistance of GF, make these devices excellent candidates for heat dissipation and pave the way to the development of GF-based cooling devices, which could efficiently dissipate heat from electronic components without requiring a forced coolant flow.

Acknowledgements

The authors thank Dr. Yoav Green for his valuable input.

References

[1] Dang, B.; Bakir, M. S.; Sekar, D. C.; King, C. R., Jr.; Meindl, J. D. Integrated microfluidic cooling and interconnects for 2D and 3D chips. *IEEE Trans. Adv. Packag.* **2010**, *33*, 79–87.

[2] Cook-Chennault, K. A.; Thambi, N.; Sastry, A. M. Powering MEMS portable devices—A review of non-regenerative and regenerative power supply systems with special emphasis on piezoelectric energy harvesting systems. *Smart Mater. Struct.* **2008**, *17*, 043001.

[3] Kim, H. S.; Kim, J. H.; Kim, J. A review of piezoelectric energy harvesting based on vibration. *Int. J. Precis. Eng. Manuf.* **2011**, *12*, 1129–1141.

[4] El-Kady, M. F.; Kaner, R. B. Scalable fabrication of high-power graphene micro-supercapacitors for flexible and on-chip energy storage. *Nat. Commun.* **2013**, *4*, 1475.

[5] Wang, G. P.; Zhang, L.; Zhang, J. J. A review of electrode materials for electrochemical supercapacitors. *Chem. Soc. Rev.* **2012**, *41*, 797–828.

[6] Mahajan, R.; Chiu, C. P.; Chrysler, G. Cooling a microprocessor chip. *Proc. IEEE* **2006**, *94*, 1476–1486.

[7] Yim, W. M.; Rosi, F. D. Compound tellurides and their alloys for peltier cooling-A review. *Solid State Electron.* **1972**, *15*, 1121–1140.

[8] Riffat, S. B.; Ma, X. L. Thermoelectrics: A review of present and potential applications. *Appl. Therm. Eng.* **2003**, *23*, 913–935.

[9] Hermes, C. J. L.; Barbosa, J. R., Jr. Thermodynamic comparison of Peltier, Stirling, and vapor compression portable coolers. *Appl. Energy* **2012**, *91*, 51–58.

[10] Koo, J. M.; Im, S.; Jiang, L.; Goodson, K. E. Integrated microchannel cooling for three-dimensional electronic circuit architectures. *J. Heat Transfer* **2005**, *127*, 49–58.

[11] Qu, W. L.; Siu-Ho, A. Liquid single-phase flow in an array of micro-pin-fins—Part I: Heat transfer characteristics. *J. Heat Transfer* **2008**, *130*, 122402.

[12] Liu, M. H.; Liu, D.; Xu, S.; Chen, Y. L. Experimental study on liquid flow and heat transfer in micro square pin fin heat sink. *Int. J. Heat Mass Transfer* **2011**, *54*, 5602–5611.

[13] Tullius, J. F.; Tullius, T. K.; Bayazitoglu, Y. Optimization of short micro pin fins in minichannels. *Int. J. Heat Mass Transfer* **2012**, *55*, 3921–3932.

[14] Du, X. S.; Liu, H. Y.; Mai, Y. W. Ultrafast synthesis of multifunctional N-doped graphene foam in an ethanol flame. *ACS Nano* **2016**, *10*, 453–462.

[15] Chen, Z. P.; Ren, W. C.; Gao, L. B.; Liu, B. L.; Pei, S. F.; Cheng, H. M. Three-dimensional flexible and conductive interconnected graphene networks grown by chemical vapour deposition. *Nat. Mater.* **2011**, *10*, 424–428.

[16] Reddy, S. K.; Ferry, D. B.; Misra, A. Highly compressible behavior of polymer mediated three-dimensional network of graphene foam. *RSC Adv.* **2014**, *4*, 50074–50080.

[17] Brownson, D. A. C.; Figueiredo-Filho, L. C. S.; Ji, X. B.; Gómez-Mingot, M.; Iniesta, J.; Fatibello-Filho, O.; Kampouris, D. K.; Banks, C. E. Freestanding three-dimensional graphene foam gives rise to beneficial electrochemical signatures within non-aqueous media. *J. Mater. Chem. A* **2013**, *1*, 5962–5972.

[18] Chen, Z. P.; Xu, C.; Ma, C. Q.; Ren, W. C.; Cheng, H. M. Lightweight and flexible graphene foam composites for high-performance electromagnetic interference shielding. *Adv. Mater.* **2013**, *25*, 1296–1300.

[19] Fang, H. M.; Zhao, Y. H.; Zhang, Y. F.; Ren, Y. J.; Bai, S. L. Three-dimensional graphene foam-filled elastomer composites with high thermal and mechanical properties. *ACS Appl. Mater. Interfaces* **2017**, *9*, 26447–26459.

[20] Xu, R. Q.; Lu, Y. Q.; Jiang, C. H.; Chen, J.; Mao, P.; Gao, G. H.; Zhang, L. B.; Wu, S. Facile fabrication of three-dimensional graphene foam/poly(dimethylsiloxane) composites and their potential application as strain sensor. *ACS Appl. Mater. Interfaces* **2014**, *6*, 13455–13460.

[21] Ren, H. Y.; Tang, M.; Guan, B. L.; Wang, K. X.; Yang, J. W.; Wang, F. F.; Wang, M. Z.; Shan, J. Y.; Chen, Z. L.; Wei, D. et al. Hierarchical graphene foam for efficient omnidirectional solar-thermal energy conversion. *Adv. Mater.* **2017**, *29*, 1702590.

[22] Reddy, S. K.; Ya'akobovitz, A. Electromechanical behavior of graphene foams. *Appl. Phys. Lett.* **2019**, *115*, 211902.

[23] Pettes, M. T.; Ji, H. X.; Ruoff, R. S.; Shi, L. Thermal transport in three-dimensional foam architectures of few-layer graphene and ultrathin graphite. *Nano Lett.* **2012**, *12*, 2959–2964.

[24] Zhou, M.; Lin, T. Q.; Huang, F. Q.; Zhong, Y. J.; Wang, Z.; Tang, Y. F.; Bi, H.; Wan, D. Y.; Lin, J. H. Highly conductive porous graphene/ceramic composites for heat transfer and thermal energy storage. *Adv. Funct. Mater.* **2013**, *23*, 2263–2269.

[25] Zhang X. F.; Yeung, K. K.; Gao, Z. L.; Li, J. K.; Sun, H. Y.; Xu, H. S.; Zhang K.; Zhang, M.; Chen, Z. B.; Yuen, M. M. F. et al. Exceptional thermal interface properties of a three-dimensional graphene foam. *Carbon* **2014**, *66*, 201–209.

[26] Cohen, Y.; Reddy, S. K.; Ben-Shimon, Y.; Ya'akobovitz, A. Height and morphology dependent heat dissipation of vertically aligned carbon nanotubes. *Nanotechnology* **2019**, *30*, 505905.

[27] Ya'akobovitz, A. Multiple thermal transitions and anisotropic thermal expansions of vertically aligned carbon nanotubes. *J. Appl. Phys.* **2016**, *120*, 165110.